Naitong LIU, Changyong JIANG, Lixi HUANG and Chen WANG (2021). Effect of porous casing on small axial-flow fan noise. *Applied Acoustics.*

doi:10.1016/j.apacoust.2020.107808

Effect of porous casing on small axial-flow fan noise

Naitong LIU

Changyong JIANG

Lixi HUANG

Chen WANG

Submitted to *Applied Acoustics* March 17 2020

Accepted November 24 2020

Effect of porous casing on small axial-flow fan noise

ABSTRACT

A novel casing treatment is studied to suppress the tip leakage vortex and postpone stall inception, leading to significant noise reduction. The new casing is made by open-cell metal foam, and its effect on both aerodynamic and acoustic performance of an axial-flow fan is investigated experimentally. As much as 10 dBA noise reduction is achieved, in the otherwise stalled flow condition. The mechanism is qualitatively analyzed by computational fluid dynamic simulations for three-dimensional, transient flow. It is found that, with the porous casing, the strength of tip leakage vortex decreases mainly because of the suppression of the pressure difference between the pressure side and suction side of the blade and the flow momentum transport at fluid-porous interface. By experimenting with different casing surfaces, the roughness of the porous casing is found not to be responsible for the delay of stall. Moreover, direct sound absorption by the porous casing is found to be negligible due to the limited volume of metal foam. The working mechanism is thus identified as purely aerodynamic.

KEYWORDS

Small axial-flow fan

Passive noise control

Tip leakage flow

Stall inception

1. INTRODUCTION

Nowadays, increasing importance has been attached to the noise problem of turbomachinery. Aerodynamic noise sources of an axial fan include the interaction between the upstream turbulence and the rotor blades, the interaction between the rotor and the stator, the tip leakage flow, the boundary layer on the surface of the blades and shroud, etc [1,2]. The present study focuses on the suppression of noise from small axial-flow cooling fans which features severe tip leakage flows. The tip clearance noise is produced by pressure fluctuations on the blade surfaces induced by the unsteady tip-leakage flow [3]. Moreover, the interaction between the tip vortices and the downstream stator vanes is also regarded as one of potential noise sources [4]. In addition to extra noise generation, fan tip leakage flow also causes significant aerodynamic loss: for instance, it may account for as much as 45% of aerodynamic losses in rotor and 30% of total losses for a typical high-pressure turbine [5]. It is well-known that a smaller tip gap is beneficial to both aerodynamic and acoustic performance of a fan [6]. However, there is always a minimum clearance being restricted by material thermal and mechanical properties, machining and installation tolerances, etc.

With a given tip clearance, there are usually two methods to reduce the noise induced by the tip leakage flow: blade modification and casing treatment. For the blade modification, installing an end-plate as an anti-vortex appendage was investigated [7]. It was found that an elaborate end-plate enhanced the fan efficiency, and the radiated aerodynamic noise was decreased by a large amount. In addition, rotating ring-shroud attached to the fan tips, which was proposed earlier by Longhouse [3], can be regarded as a special kind of circumferential end-plate and the total noise reduction was as much as 12 dB. Beside the use of end-plates, blade with end-bending [8], blade tip surface groove [9] and blade with porous tip [10] were studied in the category of blade modification.

In terms of casing treatment, Kameier and Neise [6] inserted a turbulence generator (Velcro tape, 2mm in thickness) into the tip clearance of a fan. The axial width of the turbulence generator was 6.6% of the fan radius and it extended from the upstream of the rotor to the maximum thickness of the blade profile. Both static pressure rise and fan efficiency were improved, and the stall inception was postponed simultaneously. Significant noise reduction was also obtained. It was assumed that the turbulence generator improved the energy exchange between the low-momentum fluid particles at the wall and the main flow. However, there was no unequivocal evidence for this hypothesis. As a matter of fact, the turbulence generator decreased the tip clearance locally and it definitely obstructed the secondary flow through the tip gap.

With constant minimum tip clearance, one of the most common casing treatment methods is the usage of grooves or slots on the inner wall of the casing [11], which has already been applied in large-scaled axial fans. With appropriate grooves or slots, the stall margin is improved significantly and the noise is reduced simultaneously [12-14]. Smith and Cumpsty [15] pointed out that the main working mechanism lay in the selective removal of high absolute-swirl, high-loss fluid near the trailing edge, instead of the unsteady flow effects in the slots.

Instead of making slots or grooves, the present study proposes a new approach, which is the lining of the casing wall by open-cell porous metal foams. The proposed method is inspired by the previous works of Sutliff et al [16-18]. The type of metal foam is widely used in applications such as heat exchangers, energy absorption, flow diffusion, and lightweight optics. In terms of the noise control for turbomachinery, the metal foam is applied not only to suppress the unsteady response due to fluid-structure interaction, but also as sound absorption material. Xu and Mao [19] placed a chunk of open-cell metal foam at the volute tongue of a centrifugal fan, achieving around 5 dBA noise reduction, with a tiny sacrifice of static pressure rise. It stated that the noise source strength was decreased mainly because of the suppression

of the periodic impeller-tongue interaction. Sutliff et al. [16,17] investigated the effect of metal foam layers located on different parts of the casing of a low-speed, ultra-low pressure ratio fan (4-ft in diameter). The thickness of the metal foam layer reached 2 inches. With quite low aerodynamic loss, significant noise absorption was observed when the foam metal liner in the casing was directly over the rotor. Measurement by hot films detected stronger tip vortex and the reason was supposed to be the extra path (provided by the porous zone) for leakage flow, deteriorating the fan tip flow field. Therefore, the working mechanism of this liner was purely acoustic, which differed from the thin porous casing layer proposed in the current study. The above work was extended by Sutliff *et al.* [18], which designed foam metal liners for a high-speed turbofan engine. As much as 2.5 dB noise reduction was demonstrated with 1-2% aerodynamic performance loss at the design condition. The working mechanism was supposed to be similar with that being proposed in the study of low-speed fan.

The goal of the present work is twofold. One is to quantify the improvement of aerodynamic performance and the noise reduction of a small axial-flow cooling fan with the porous casing experimentally. The other is to investigate the working mechanism. Totally there are three hypothetical mechanisms being proposed: (i) sound absorption by porous material, (ii) the influence of the roughness of metal foam and (iii) the interaction between the fan tip leakage flow and the porous zone of the casing. The first is roughly estimated by numerical simulation through COMSOL with no consideration of the effect of fluid flow, and the aerodynamic noise source is approximately assumed as an axial dipole on each rotor blade. The effect of the roughness of the porous casing surface is evaluated experimentally by attached air-tight sand paper on the casing. The aerodynamic effect of the porous zone on the tip leakage flow is investigated through computational fluid dynamic (CFD) by CFX. In terms of the choice of turbulence model, k-ω shear-stress-transport (SST), Baldwin-Lomax turbulence model and large eddy simulation had already been proved to be able to give a satisfactory prediction of the fan overall performance and tip flow

structure [20-25]. Moreau and Sanjose [26] made a careful investigation on the different kinds of CFD method for a ring fan. The work found that the unsteady methods, including unsteady k-ω SST, SST-scale adaptive simulation as well as lattice Boltzmann method, offers not only a better prediction of the fan overall performance (at lower flow rate), but also a more precise structure and the dynamics of the turbulent vortices in fan tip flow than the steady RANS. In the present study, unsteady RANS type k-ω SST turbulence model is applied and the fluid is assumed to be incompressible.

The remainder of the present paper is structured as follows: a brief description of the experimental setup is firstly given, followed by the experimental comparison of original rigid casing and the porous casing on both aerodynamic and acoustic characteristics of the tested fan. Subsequently, the hypothetical working mechanisms mentioned above are investigated in the following three sections. At last, conclusions are presented.

2. Experimental setup

2.1 The sample small axial-flow cooling fan

As shown in Fig. 1, the test sample fan consists of a rotor, a casing and an inlet bell-mouth. The rotor comprises 7 blades and it is produced by rapid prototyping. The blade is designed according to the velocity triangle method [27]. Table 1 lists the detailed design specifications of the rotor. According to the work of Tyler and Sofrin [28], the mismatch index of the rotor-stator interaction noise is defined as $\nu = mB - kS$, where B and S are the numbers of rotor blades and struts, respectively, m is the order of blade passing frequency and k is any integer. Huang [29] pointed out that $|\nu|$ should be ideally 2 or above to avoid loud discrete noise for small axial-flow fans for the first few (m=1,2,3) blade passing frequencies. In this case, B=7 and S=5， which manages to keep ν at 2 when m=1 and k=1. In addition, the diameter of struts should not be very large in order to avoid excessive flow blockage hence noise radiation [30],

while at the same time it has to provide adequate structural strength. In this work, the cylindrical strut diameter is 3 mm and its aerodynamic noise is neglected in the following analysis. The tip clearance is 1.2 mm as specified by the commercial products of this class. During the experiment, the fan is powered by a 48V DC electrical source and the rotational speed is controlled by a signal generator. The rotational speed of the motor has negligible variation (± 5 r/min) with the loading during experiment.

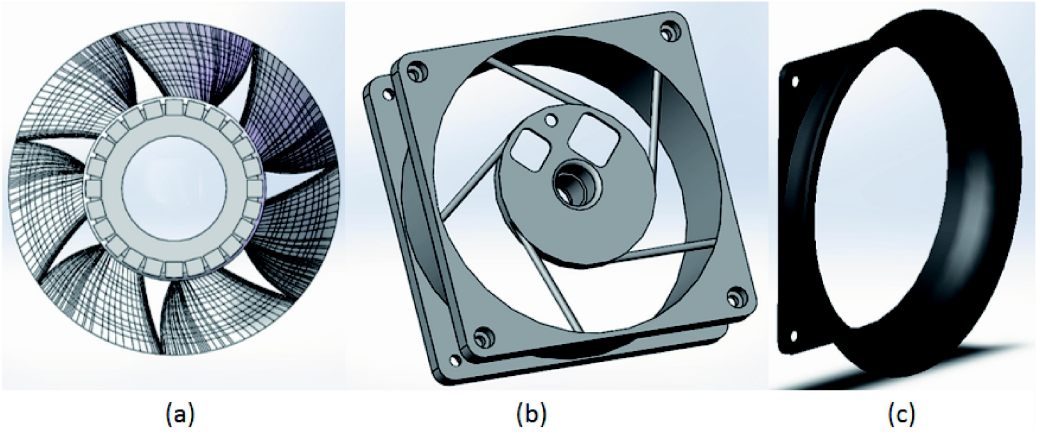

Fig. 1. Profiles of (a) 7-blade rotor, (b) 5-strut casing and (c) inlet bellmouth of the tested fan.

Table 1. Design specifications of the rotor.

Tip diameter (*d*)	113.6 mm
Hub diameter	63.0 mm
Number of blades (*B*)	7
Tip stagger angle	62.0°
Tip chord length	51.3 mm
Hub stagger angle	30.6°
Hub chord length	28.0 mm
Axial chord length (C_a)	31.0 mm
Designed rotational speed (Ω)	3660 rpm

The fan with untreated rigid casing is regarded as the baseline. For the treated fan casing, Nickel and Copper foam layers of 3 mm in thickness are studied. Their characteristics are listed in Table 2 and they are identified as PC1 and PC2 (PC: Porous Casing), respectively in the following plot legends. The metal foam layer is

attached closely on the inner wall of treated casing which has a larger inner radius of 61 mm, so as to keep a smooth duct passage and a constant tip clearance of 1.2 mm. Moreover, the small heaves of the porous casing wall are evened out by complete revolutions of a metal rotor whose tip radius is 58 mm with a machining error of less than 0.05mm. Figure 2 gives the front view of the tested fan and its close-up with key annotations.

Table 2. Characteristics of two kinds of metal foam materials.

	Material	**Thickness**	**Porosity**	**Standard**	**Aperture Diameter**
PC1	Nickel	3 mm	98%	100 PPI	0.2 mm
PC2	Copper	3 mm	95%	130 PPI	0.1 mm

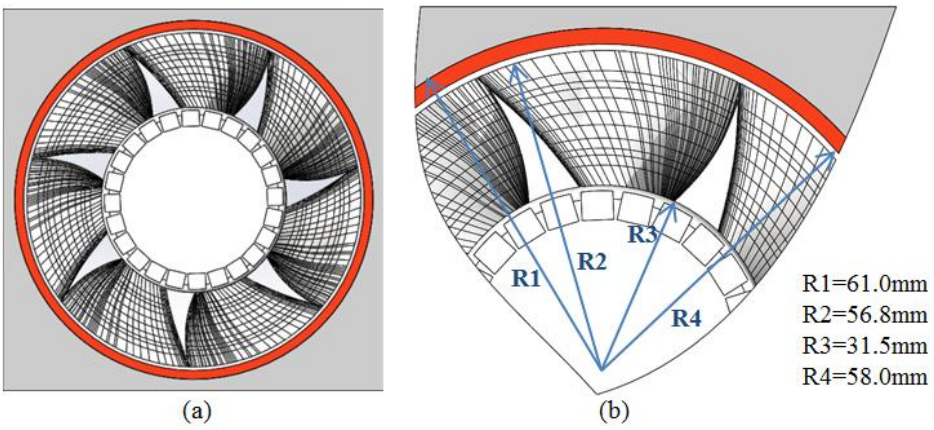

Fig. 2. (a) The front view of the tested fan, and (b) its close-up with annotations of radii for the blade hub and tip, the original casing and the casing with metal foam layers (in red).

2.2 Measurement of aerodynamic and acoustic performance

To realize both functions of aerodynamic and acoustic performance measurement, a sound-absorbing fan test rig has been built and it is located in a full anechoic chamber. This test rig is designed by referring to the one in the previous study [31] and they both are built in strict accordance to the ANSI/AMCA Standard 210 [32]. The ductwork for aerodynamic measurement is illustrated in Fig. 3, while the acoustic

measurement is demonstrated in Fig. 4. As shown in Fig. 3, sound absorbing fibers are filled in the large steel tube and the duct inner wall (diameter: 0.12 m) is lined with perforated panels allowing the noise to penetrate into the fibers and get absorbed while keeping the flow in the central passage. In the experiment, the test fan is located at the inlet (left-hand-side) of the set-up. The turbulence in the blowing flow is rectified by a flow straightener, which is located at the position of 0.54 m downstream of the fan outlet. The flow straightener is composed of many small square cells of 0.075D in side length, 0.005D in thickness and 0.45D in axial depth. The Pitot tube (being located at 1.605 m downstream of the fan outlet) measures the total pressure and the flow speed, while a downstream valve adjusts the flow rate. The static pressure rise across the test fan, ΔP, and the total volume flow rate, Q, are obtained following the standard ANSI/AMCA procedures.

As shown in Fig. 4, the sound radiated by the fan outside the duct is measured by three 1/4-inch microphones at three angular locations on the arc of 0.8 m radius from the center of the rotor, while the sound radiated into the duct and the noise of the valve is considered totally absorbed by the duct lining with no effect on the measurement. The microphones are powered by a B&K Nexus conditioning amplifier (type: 2960) and the output electrical signal are sampled by an A/D DAQ cards (NI USB-6251) at 51.2 kHz and then processed in PC with MATLAB. A tachometer is also used to monitor the fan rotational speed. Each acoustic measurement is taken for 20 seconds. The sound energies from the three angular positions (0°, 45°, 90°) are averaged to obtain the sound pressure spectrum and level of any particular aerodynamic operation point.

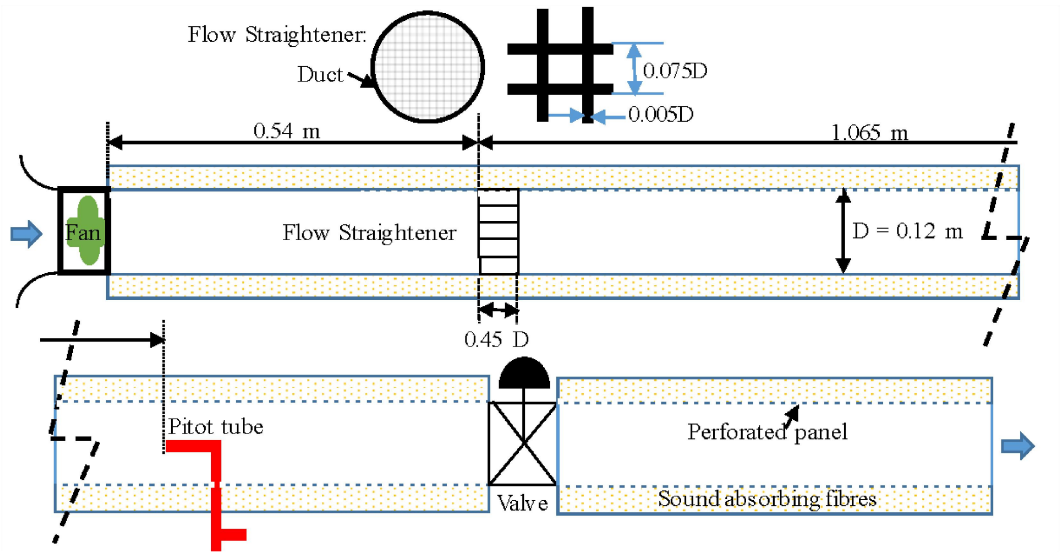

Fig. 3.Sketch of the ductwork and details of flow straightener for the aerodynamic measurement.

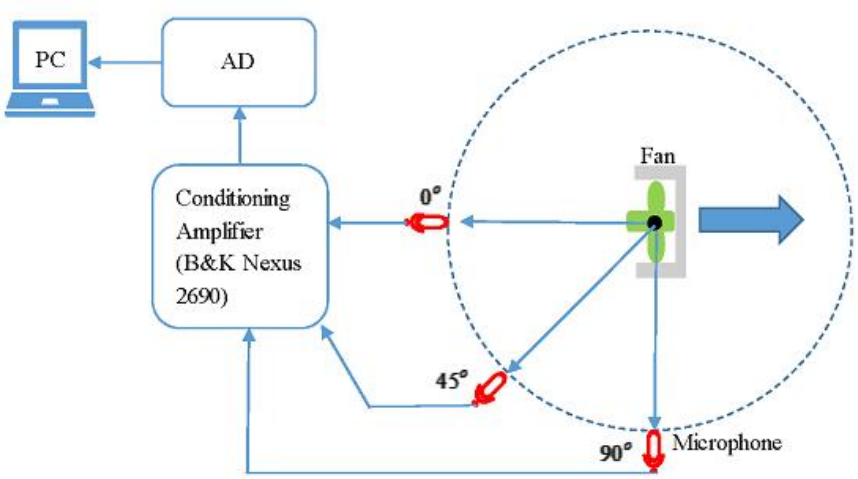

Fig. 4.Noise measurement set-up.

3. Main experimental results

The experimental results for both aerodynamic and acoustic performance of fan are presented in this section. Preliminary analyses of the effect of the rough surface of the foam casing and the direct sound absorption are also considered.

3.1 Comparisons of the P-Q curves and the radiated noise

Figure 5 compares both aerodynamic and acoustic performance between the fan with original rigid casing (labelled as “Baseline”) and the ones with porous casings

(labelled as “PC1” for Nickle foam casing and “PC2” for Copper foam casing). As shown in Fig. 5(a), the baseline suffers from a stall in the volume flow rate (Q) range of 60 to 100 CFM. During stall, severe boundary layer separation takes place. Simultaneously, the pressure rise no longer increases with reducing Q and falls off instead, followed by dramatic noise increase. On the P-Q curve, the stall region features a significant dip in the static pressure. When porous casings are applied, the aerodynamic performance is improved significantly with a recovery of 15-20 Pa static pressure rise in the stall region. Stall inception is postponed, from $Q \approx 98$ CFM to $Q \approx 65$ CFM for PC1 and $Q \approx 75$ CFM for PC2. It is noted that the porous casing does not introduce much effect in the flow regime outside stall.

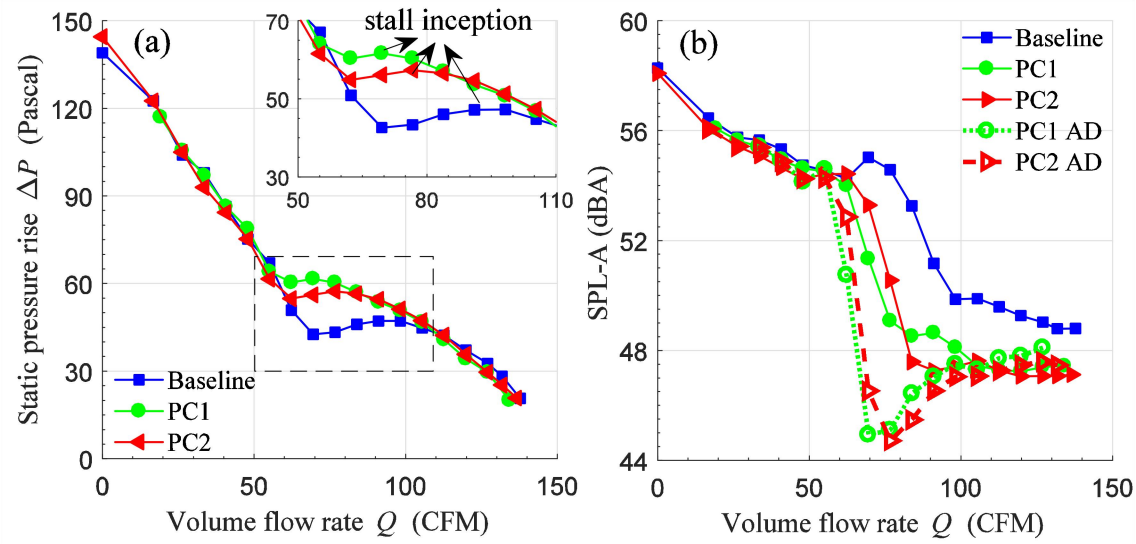

Fig. 5. Comparisons of (a) the P-Q curves and its zoom-in of stall region and (b) A-weighted SPL among fans with rigid casing (Baseline), Nickel foam casing (PC1) and Copper foam casing (PC2), respectively, measured at the baseline rotational speed of 3660 rpm and the same operating conditions at the adjusted speeds (denoted by “AD” in legend).

Noise comparison is made in Fig. 5(b). The SPL-A (A-weighted Sound Pressure Level) curves for both “PC1” and “PC2” are measured at the same design rotational speed as baseline case. Two more curves are presented, and they are labelled “PC1 AD” and “PC2 AD”, respectively, where “AD” stands for adjusting the rotational speed. Since casing treatment improves the aerodynamic performance near the stall

region, they are obtained when the fan rotational speed is reduced for the casing-treated fans in order to deliver the identical flow rate and pressure rise as the baseline. Significant noise reduction is obtained, for both the same and reduced fan rotational speeds, in the range of volume flow rate $Q > 60$ CFM. It is noted that the curve for PC2 shows more noise abatement when $Q > 80$ CFM, while PC1 performs better when Q is in the range of 60 to 80 CFM. When compared at the same aerodynamic working conditions by adjusting the rotational speed ("PC1 AD" and "PC2 AD"), more noise reduction is logically achieved. The maximum noise reduction is about 10 dBA at $Q \approx 70$ CFM, where the P-Q curve of the baseline reaches its valley in stall.

Figure 6 compares the spectra and the accumulative sound energy spectra when the volume flow rate of the baseline is Q_{Baseline}=120 CFM (Fig.6(a) and (c), before stall inception) and Q_{Baseline}=76 CFM (Fig.6(b) and (d), when stall takes place for baseline), respectively. In each figure, "PC2" refers to the fan with Copper foam casing sharing the identical rotational speed with the baseline, and "PC2 AD" means the casing treated fan operating at the same operation condition of the baseline at adjusted speed. In terms of the accumulative sound energy spectrum, it is defined as

$$E(f_{\text{i}}) = \int_0^{f_{\text{i}}} p^2(f)\,\mathrm{d}f \tag{1}$$

where $p^2(f)$ is the power spectral density of received acoustic pressure. The spectrum for E is normally smooth and its slope $\mathrm{d}E/\mathrm{d}f$ helps to identify the major energy contributions in a way better than the standard logarithmic spectrum without the energy integral treatment. The tonal noise is identified by the narrow frequency bands around BPF (blade passing frequency) and its harmonics. A-weighting is applied before the sound energy integration. From Fig.6(a) and (c), the noise reduction is mild before stall inception. There is no clear discrepancy between the baseline and PC2 in their broadband spectra (Fig. 6(a)), while the tonal noise (especially around BPF=427 Hz as well as 5×BPF=2135 Hz) decreases with the treated casing. Since porous casing does not improve the aerodynamic performance of

the fan significantly before stall, the variation of the rotational speed is slight which causes little noise reduction of PC2 AD. When stall takes place, with the identical speed, the suppression of the total noise is very impressive mainly because the broadband of PC2 decreases significantly before 4000Hz (Fig. 6(b)), instead of the suppression of the tonal noise (Fig. 6(d)). PC2 AD radiates even lower noise due to the significant reduced rotational speed because of the delay of the onset of stall.

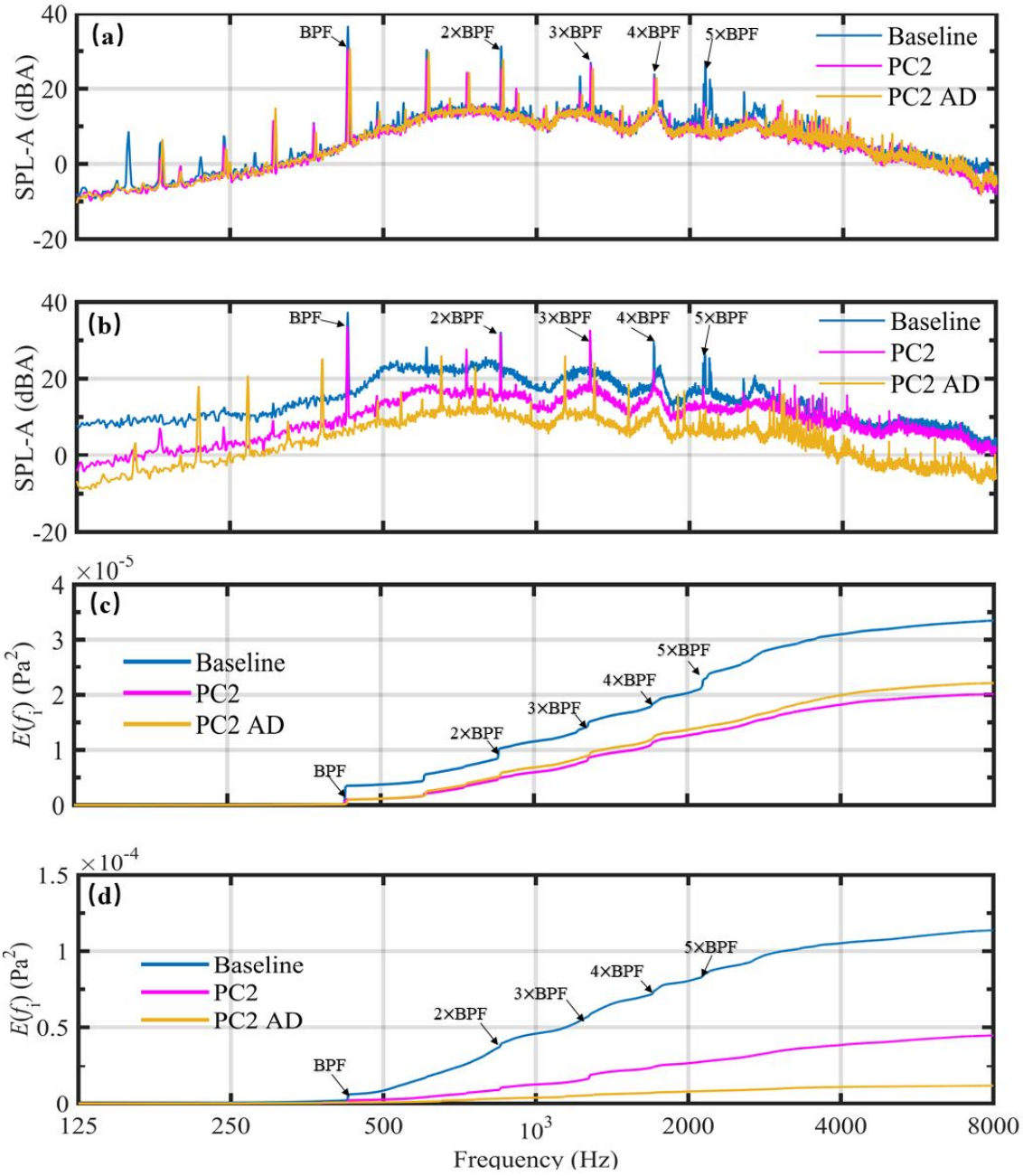

Fig.6. Comparisons of (a, b) the spectra and (c, d) the accumulative sound energy spectra among the fan with rigid casing (Baseline), the fan with Copper foam casing working at the identical rotational speed of the baseline (PC2), and the casing treated

fan sharing the same operating condition with the baseline at the adjusted speed (PC2-AD). (a) and (c) are measured at Q_{Baseline}=120 CFM (before stall inception). (b) and (d) are measured at Q_{Baseline}=76 CFM (in stall).

3.2 Sound absorbing directly by attached porous material

One of the possible mechanisms for the reduction of fan noise radiation is the direct sound absorption by the open-cell metal foam. To roughly estimate this absorptive effect, acoustic simulation is conducted with commercial finite element software COMSOL Multiphysics. A simplified model including a rotor with an axial dipole noise source attached on each blade is proposed.

The acoustic properties of the metal foam layer (Copper foam in this case) are measured in an impedance tube, using the two-cavity method proposed by Utsuno et al. [33]. With this method, the equivalent wavenumber and characteristic impedance of the metal foam are obtained. After curving fitting with Delany and Bezely's empirical formula [34], the flow resistivity of the experimented metal foam is estimated as $18000\,\text{Pa}\cdot\text{s}/m^2$, which is further imported into COMSOL for simulation.

The entire simulation domain is shown in Fig. 7(a). The fan is installed at the inlet of a straight flow tube. All the boundaries of the fan are set as rigid walls and an axial dipole noise source is set on each blade of the fan. The exit of the flow tube is set as non-reflection boundary. In order to investigate the inlet noise radiation property, a semi-spherical radiation domain with a so-called Perfect Match Layer (PML) is used [35]. The base of the semi-spherical domain is set as rigid wall to simulate the condition of a flange for ease of computation and it is not expected to make any significant changes to the absorption capability of the casing layer.

In this case, the metal foam is set as a rigid frame porous material, without considering the vibration effect of the skeleton. When the skeleton vibration cannot be neglected, the Biot's model needs to be applied [36-37]. The total radiated acoustic energy from the inlet is integrated on the surface of the semi-spherical domain. The

total radiated noise from the fan with and without porous casing are compared in Fig. 7(b). The noise absorption effect is negligible in the low frequency region under 2.5 kHz (less than 1 dB).

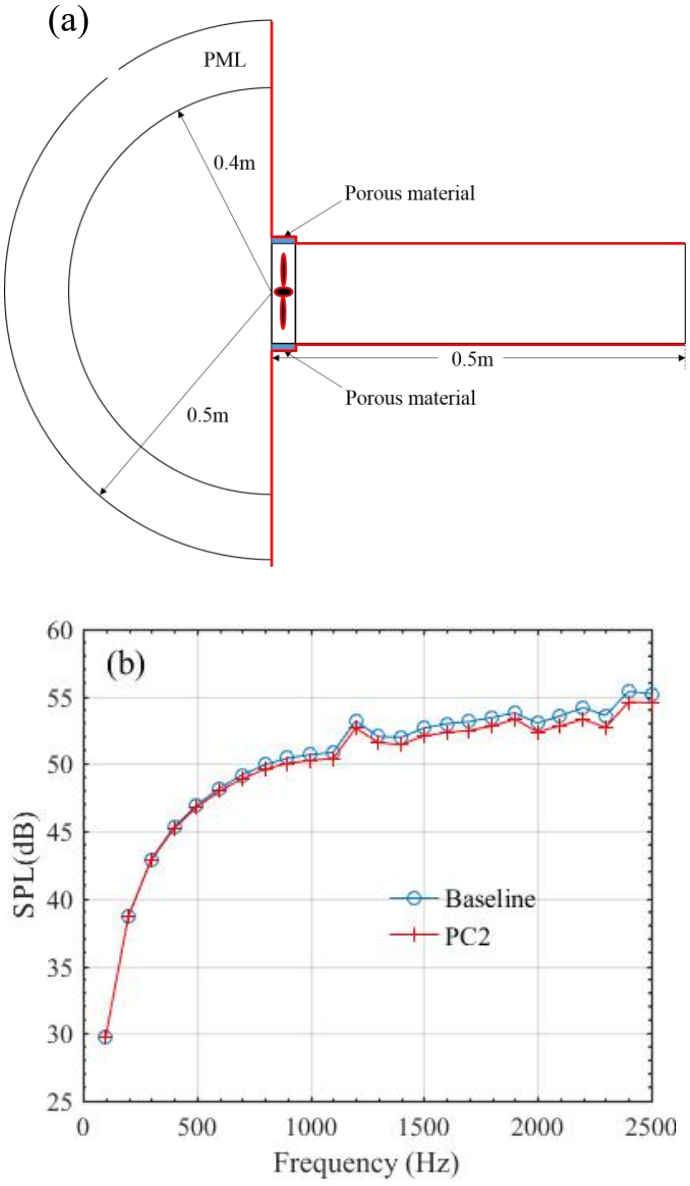

Fig 7. Schematic of (a) full simulation domain in COMSOL for the sound absorption by the porous casing (red: acoustic rigid surface) and (b) the comparison of total radiated noise with/without casing treatment.

Note that the present conclusion seems to be much different from that of Sutliff *et al.* [16,17] which said that the acoustic attenuation effect of the metal foam liner plays the most important role in the fan total noise reduction. Actually, in Sutliff *et al.*

[16,17], the fan rotated with low aerodynamic loading but there is no information about the effect of metal foam liner when the fan works near stall. Although the present investigation focuses on ruling out the possibility that direct sound absorption dominates for the noise abatement when the fan works near stall, it also finds noise reduction (around 1 dBA) when the aerodynamic loading is low (the value of Q is high), as shown in Fig. 5(b). However, this noise reduction cannot compare with that in Sutliff *et al.* [16,17]. The main reason is supposed to be that, the volume of the metal foam liner (3 mm in thickness and 31 mm in axial length) in the present work is limited compared with that in Sutliff *et al.* [16,17] (2 inch in thickness and 9 inch in axial length).

3.3 Effect of the casing surface roughness

One hypothetical reason for the delay of stall inception is the interaction between the rough surface of casing and fan tip flow. Rao *et al.* [38] experimentally compared the performance of a turbine rotor working with smooth surface casing and rough surface casing (by attaching sandpaper), respectively. Using rough-surface casing, the weakened tip vortex system was clearly observed: the tip leakage vortices were reduced in size and there was less pressure loss detected within the vortices. It is argued that these changes are beneficial to postpone stall inception. However, there was no noise comparison in this work.

The possibility that the rough surface of metal foam is responsible for the aerodynamic gain is put to test by using an air-tight abrasive paper on the inner wall of the casing in the present work. This configuration is illustrated in Fig. 8 (a) and a photo of the paper in test is shown in Fig. 8(b). The maximum thickness of the abrasive paper is 0.6 mm and the minimum tip clearance size is kept at 1.2 mm.

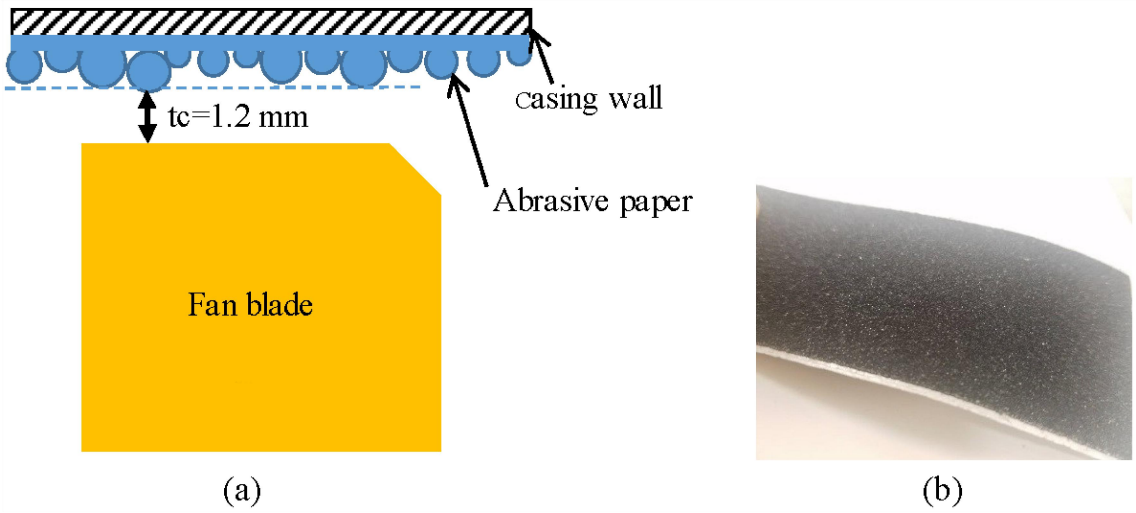

Fig. 8. (a) Sketch of casing attached by abrasive paper and (b) a photo of the abrasive paper in test.

Aerodynamic characteristics of the fans with smooth casing (labelled as 'Baseline'), porous casing (labelled as "PC1") and rough-surface casing attached by abrasive paper are compared in Fig. 9. There is tiny difference among the three P-Q curves when Q>100 CFM (before stall inception of baseline) and Q<50 CFM (after stall). However, when the original casing is replaced with the rough one, the onset of stall is postponed from about $Q \approx 98$ CFM to $Q \approx 85$ CFM. In addition, ΔP gains a little when Q is in the range of 60 to 100 CFM with the maximum enhancement approximately being 8 Pa. Nevertheless, the aerodynamic improvement brought by rough surface cannot compare with that of porous casing (PC1 for instance) which contributes to up to 20 Pa static pressure increase.

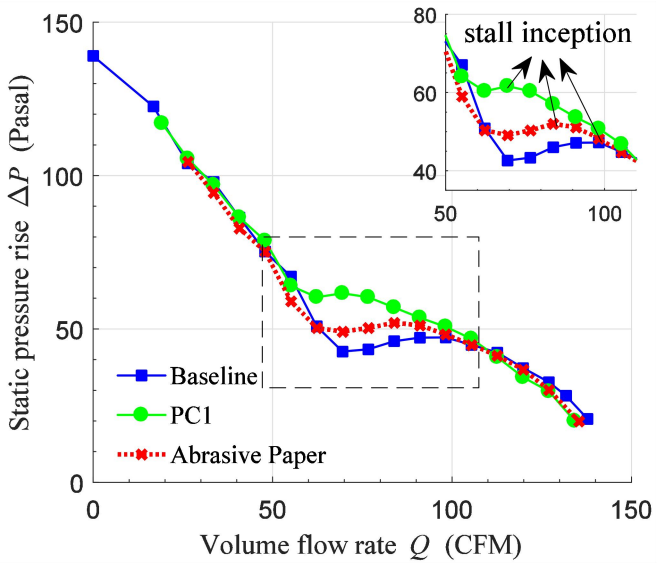

Fig. 9. Comparison of the P-Q curves for the fans with smooth casing (the baseline), Nickel foam porous casing (PC1) and the rough surface casing with the abrasive paper.

Figure 10 compares the total noise and the broadband component of the above three fans with identical rotational speed 3660 rpm. From Fig. 10(a), unlike PC1, the total noise radiated from rough surface casing increases when compared with the baseline. Figure 10(b) shows that the broadband noise of rough surface casing is almost the same as that of the baseline and it even decreases a little (less than 1 dBA) when Q is in the range of 60 to 90 CFM. However, this reduction of the broadband noise for the rough surface casing is insignificant when compared with that of PC1. Therefore, it can be deduced that tonal noise is increased with the rough casing surface. During the experiment, the abrasive paper band is attached closely on the circular inner wall of casing, and there leaves an axial fissure at the joint of two ends of the paper band. The interaction between the rotating blades and the fissure is supposed to be the main source of the extra tonal noise. Moreover, blockage by the arbitrary distributed sand particles on the abrasive paper is also supposed to be a potential reason.

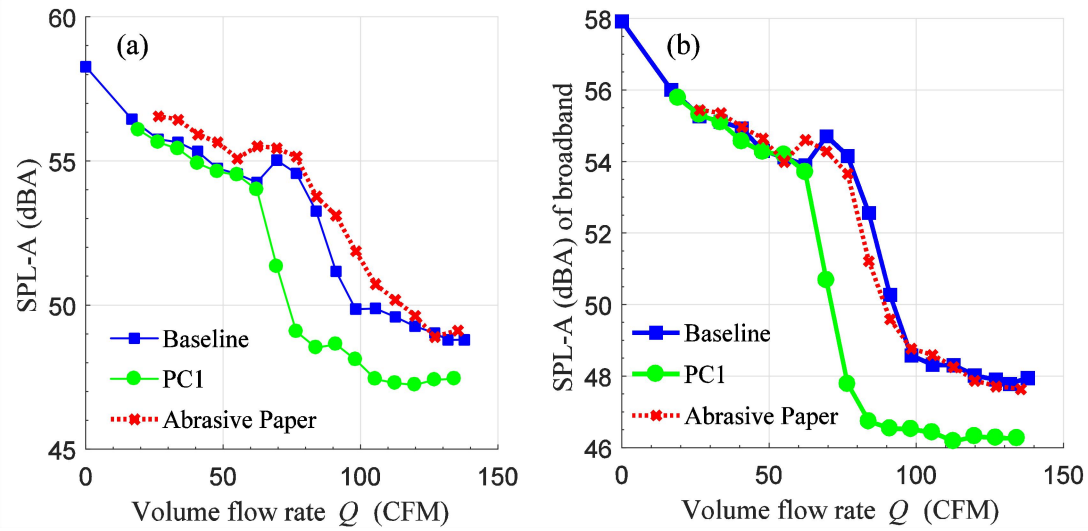

Fig. 10. Comparisons of (a) the total noise and (b) the broadband noise for the fans with smooth rigid casing (baseline), Nickel foam casing (PC1) and the rough casing with abrasive paper, all at the rotational speed of 3660 rpm.

To conclude, although rough casing surface benefits the fan aerodynamic performance a little, the total noise increases. Consequently, the impressive noise reduction achieved by PC1 and PC2 is not mainly due to the rough surface characteristic of the attached porous material, but the porous zone behind the coarse boundary.

4. Aerodynamic analysis by numerical simulation

To understand the aerodynamic effect of the porous zone behind the casing surface on the tip flow, a three-dimensional, transient-flow numerical simulation is carried out by the commercial computational fluid dynamic software ANSYS CFX. In CFX, Navier-Stokes equation is solved by finite volume method [39]. The flow fields of the baseline and the fan with porous casing are compared.

Note that the qualitative explanation of the effect of the porous casing on delay of stall inception and the resulting noise reduction is the top priority in this work, instead of accurate prediction of the fan performance. In view of this, some simplifications and approximations are conducted for the convenience of grid generation and saving time, which include

(1) There is only one single blade channel in the numerical simulation and periodic boundary conditions are imposed along the boundaries in the pitch-wise direction (highlighted by lines '1' and '2' in Fig. 11(a)).

(2) Downstream thin supporting struts are not considered as their influence on the tip-leakage flow near the blades is unlikely to be significant.

(3) The bellmouth is removed while the inlet channel is extended. Moreover, the hub is extended at its both ends, to the boundaries of the whole computational domain, as shown in Fig. 11(b).

(4) Flow in the porous zone is calculated through solving Navier-Stokes equation combining with the volume-averaged model. The volume-averaged model generates two additional terms, namely Darcy term and Forchheimer term, which are added to the original momentum equation for describing the momentum loss due to the porous material [40]. For homogenous porous material (no gradient model term), the porous momentum loss model can be formulated as follows:

$$-\frac{P_s}{dx} = \frac{\mu}{K_p}U + K_L\frac{\rho}{2}U^2 = C_{R1}U + C_{R2}U^2 \quad (2)$$

where P_s denotes the static pressure drop across the porous zone, x represents the flow direction, μ is the dynamic viscosity coefficient, ρ is the density of fluid, U is the flow velocity, K_p is permeability and K_L is loss coefficient. In Eq.(2), $\frac{\mu}{K_p}U$ and $K_L\frac{\rho}{2}U^2$ are known as Darcy and Forchheimer term, which account for the viscous and inertial effect of the porous material, respectively. C_{R1} and C_{R2} are linear and quadratic resistance coefficients respectively, which are normally achieved experimentally through measuring the pressure drop caused by the metal foam sample in test with different air flow rate [41,42]. In the present study, fan performance test bench is implemented to achieve the flow resistance of the tested metal foam copper. As shown in Fig. 12 (a), a piece of air-tight panel, which has a rectangular through hole (Size: 300×120 mm), is fixed at the inlet of the fan

performance test bench. The metal foam copper (1.5 mm in thickness) is attached tightly to the sides of the hole. There is an inlet tube (Section size: 300 × 120 mm) made by air-tight panels is located at the upstream side of the sample and a Pitot tube is applied for collecting the static pressure. The velocity of flow through the sample would be measured when a negative static pressure is assigned. The relationship between the pressure drop (Static pressure drop $= p_{\text{in}} - p_{\text{out}}$, p_{in}: static pressure detected by the pitot tube at upstream of the sample, p_{out}: static pressure assigned by the fan performance test bench) and averaged flow velocity across the sample is demonstrated in Fig. 12 (b). $\boldsymbol{C_{R1}}$ and $\boldsymbol{C_{R2}}$ are achieved by the curve fitting for the curve in Fig. 12 (b). Details are listed in Table 3. In addition, the effect of surface roughness is not taken into consideration in numerical simulation.

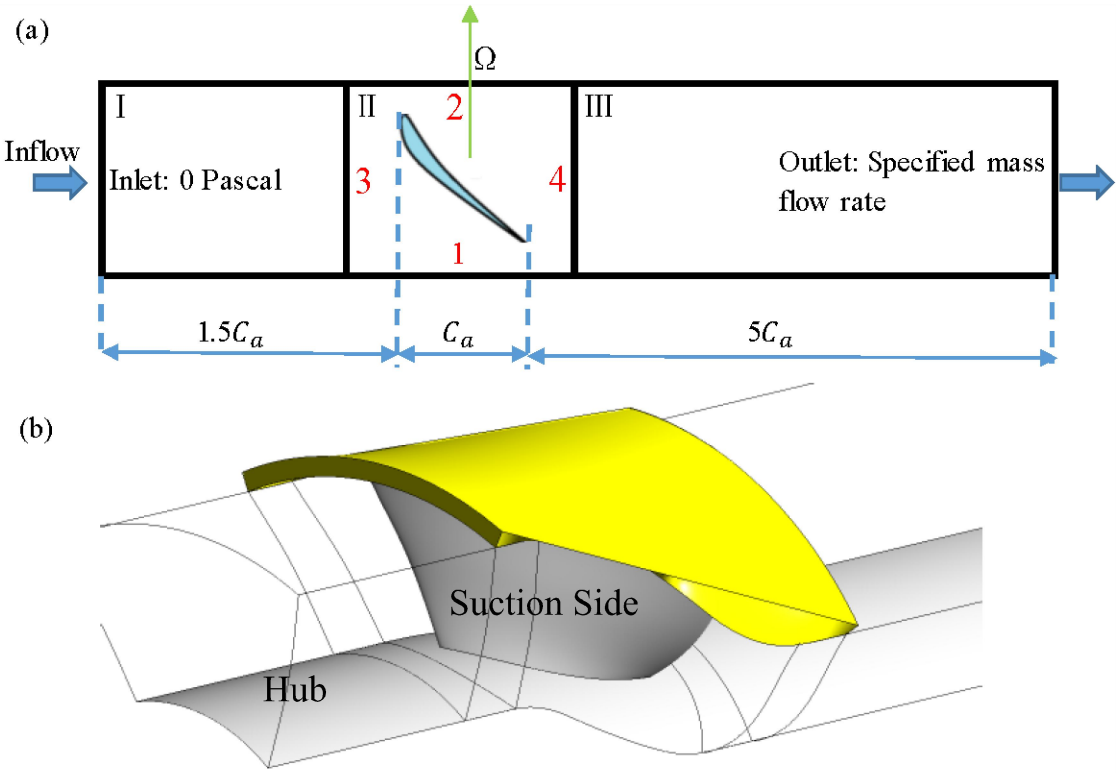

Fig. 11. Schematic of (a) full computational domain with key boundary conditions and annotations and (b) the highlighted porous zone (yellow) of casing treatment.

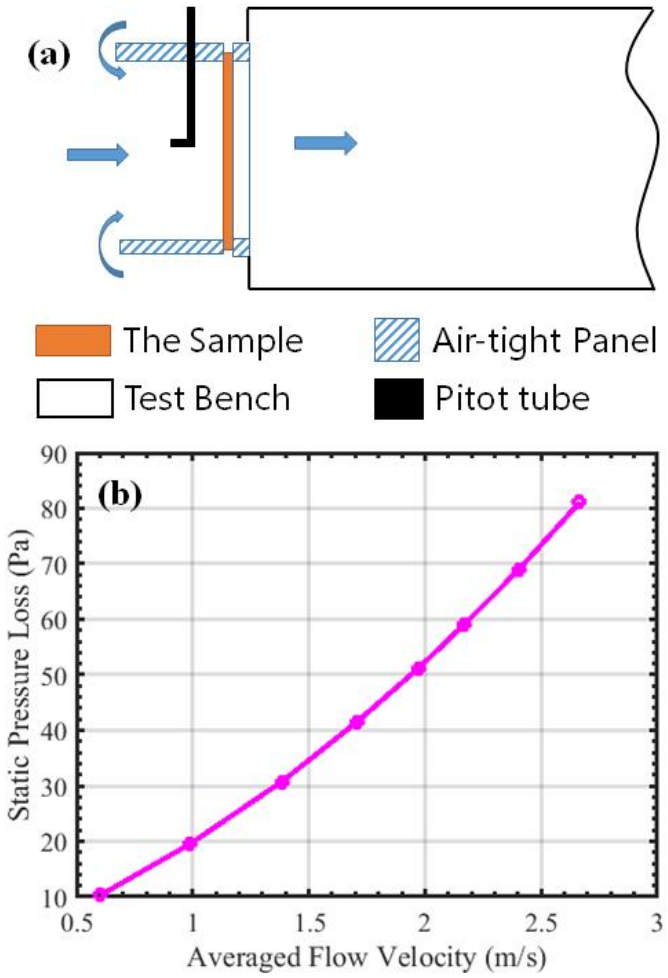

Fig. 12. (a) Schematic of the setup for the measurement of pressure drop of the metal foam and (b) the relationship between the pressure drop and the averaged flow velocity through the tested metal foam copper (1.5mm in thickness).

Table 3.Physical properties of the materials for the porous zone in the numerical simulation.

Porosity	C_{R1}	C_{R2}	**Feature**
95%	8873	4280	Isotropic

As shown in Fig. 11(a) in the side-view, the computational domain for the baseline is divided into three regions: inlet (I), rotor (II) and outlet (III). The ambient total pressure is specified at the inlet boundary while the mass flow rate is specified at the exit. The inlet boundary is at a distance of $1.5C_a$ before the leading edge (LE) of blade, while the outlet boundary is set at $5C_a$ from the trailing edge (TE). Since the

Mach number of the blade tip is only around 0.068, the change of flow density is negligible and the fluid is set to be incompressible air at 25℃. Multi-Reference Frame (MRF) is applied to simulate the rotation of blade: the fluid region of II is set in the rotating reference frame with a speed of 3660 rpm, while domains I and III are set to be stationary. For transient flow simulation, the interfaces between I and II (marked as line '3' in Fig. 11(a)), and between II and III (line '4') are set as transient sliding interfaces, which simulate the transient relative motion between two adjacent regions on each side of the interfaces and updates the interface position each time step. Surfaces of both the hub and the blades are no-slip stationary walls relative to their respective reference frames, while the shroud surface is stationary in the absolute frame. The porous zone, which is 3 mm in thickness and covers the whole shroud surface right above the blade, is highlighted as the yellow bulk in Fig. 11(b).

The structured grid is applied and the grid independence test is carried out with five mesh settings conducting 8-24 layers of mesh at an interval of 4 layers in the tip clearance zone. One example of the grid in the tip clearance region is shown in Fig. 13. The size of grid in the other computational zones is then adjusted to ensure the consistency of mesh. The number of mesh layers and the total number of grid cells are listed in Table 4. y^+ is approximately 1 for the mesh of boundary layer close to the blade. P-Q curves of the baseline fan by the five mesh settings are demonstrated in Fig. 14. There is no obvious variation on fan aerodynamic performance with more grids than Layer 16 which is thus applied in the following computation for saving computing time. For the porous casing fan, the grid dimension in the porous zone is assigned to be consistent with the grid in tip. The grid is clustered near the leading edge, trailing edge and top surface of the rotor blade.

Table 4. Mesh details of five mesh settings.

Number of layers in the tip region	8	12	16	20	24
Total number of cells $\times 10^6$	1.37	1.53	1.69	2.37	2.94

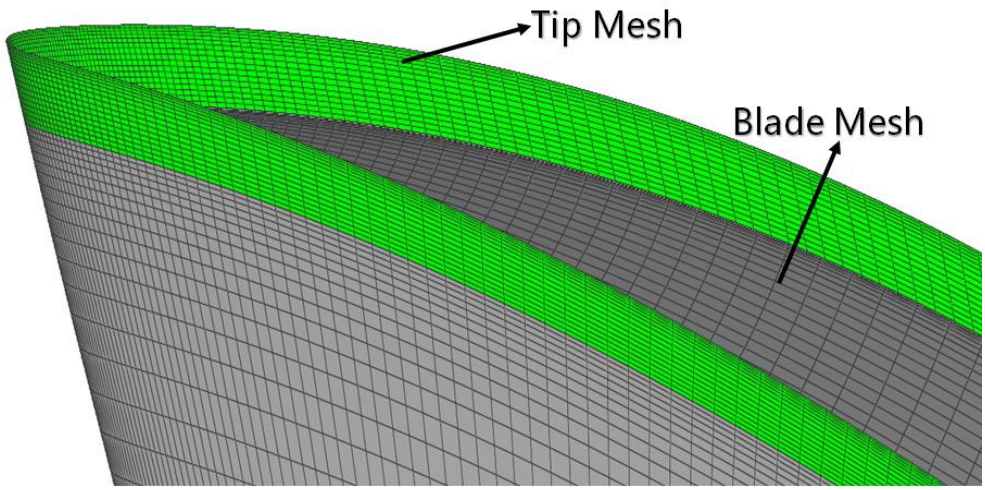

Fig. 13. Schematic of mesh details in the tip clearance region.

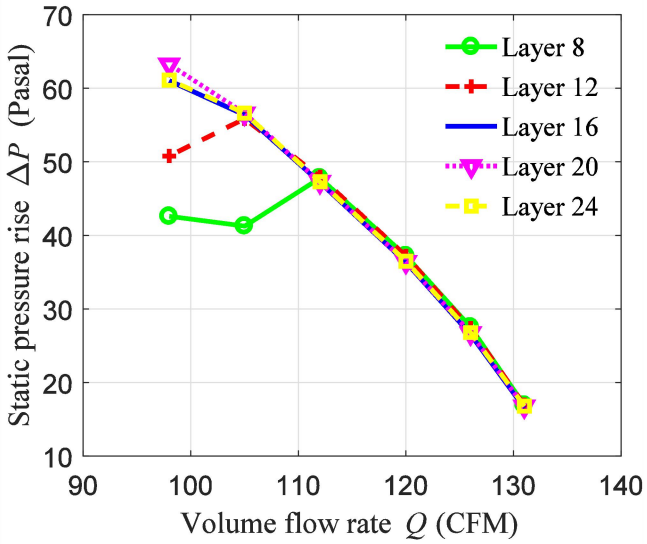

Fig. 14. Characteristic curves achieved by five mesh settings in steady simulation.

Note that the aforementioned simplifications and approximations would definitely cause discrepancy on the P-Q curves from experiments and CFD [43]. Especially, there is a significant pressure difference detected experimentally (roughly 20 Pascal) when fan operates near stall inception. Since the main purpose of the present study is observing the change of fan tip leakage vortex when porous casing is applied, such simplifications do not affect the conclusions in interest. The result is not convergent when stall takes place. Therefore, in the present study, the simulation is conducted at near-stall condition (Q = 105 CFM) to investigate the effect of porous casing on the delay of stall inception. The convergence criterion is below 10^{-5} in the

transient flow simulation. The time step for the transient flow simulation is set to be 4.55×10^{-6} sec, during which a fan blade rotates 0.1° .

Before revealing how stall inception is postponed, it is necessary to make clear the mechanism of stall for axial-flow fans. It is generally believed that when fan works close to its stall condition, the blade passage is blocked by a stagnation zone (also known as “low velocity/energy zone”) without any flow passing through [44]. This stagnation zone is generated by the accumulation of continuous upstream tip leakage flow or the breakdown of the tip leakage vortex (‘TLV’ for short) [45]. Blockage due to the stagnation zone would trigger the onset of fan rotationary stall, leading to deterioration of fan aerodynamic performance and loud noise.

Figure 15 demonstrates the streamline of tip leakage flow of the baseline and the fan with casing treatment. The streamline in Fig. 15 is colored by the value of absolute velocity of flow. Driven by the static pressure difference between the pressure side and the suction side of blade, the tip leakage flow injects upstream across the fan tip. Then, it impinges on the main flow and rolls into the tip vortex. The tip vortex moves with the main flow and interacts with the following adjacent blade at its rear part. According to Fig.15, there is no obvious difference on the appearance and trajectory of the streamline of two cases. However, the porous casing suppresses the absolute velocity of tip leakage flow (the color of the streamline turns from pale blue to dark blue). Table 5 lists the mass flow rate of the flow going through a plane (namely the ‘Plane T’) which is nearly parallel to the blade tip chord and covers the whole gap over the blade tip, as shown in Fig. 16. In addition, both mean axial velocity and mean circumferential velocity of the flow going through the Plane T are given. As shown in Table 5, both mass flow rate and the magnitude of the mean axial flow velocity decrease with porous casing. The tip leakage flow owns less momentum as it impinges on the main flow, leading to a tip vortex with lower strength [46].

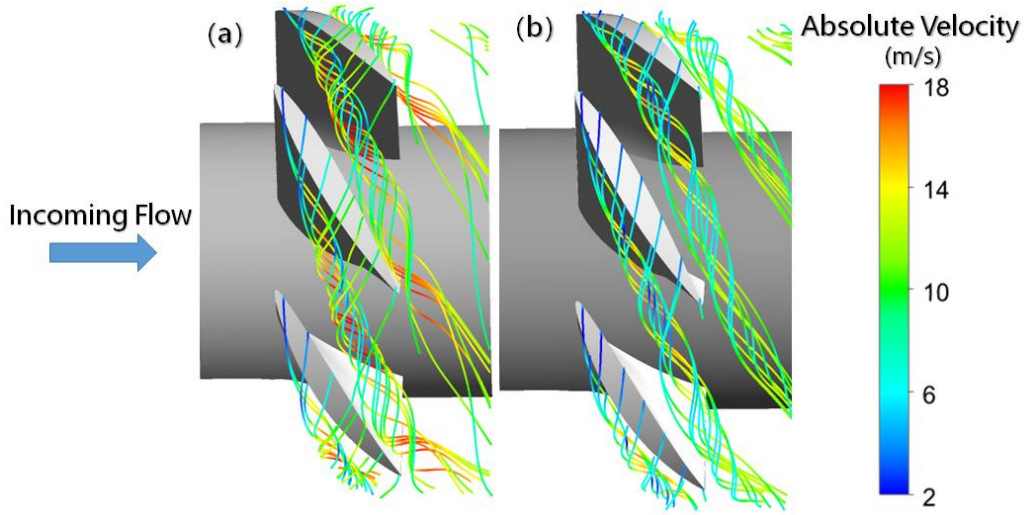

Fig. 15. Tip leakage flow of (a) the baseline and (b) the fan with porous casing. The streamline is colored by absolute velocity (Unit: m/s).

Table 5.Fluid flow through the tip gap.

	Mass Flow Rate (kg·/s)	**Mean Axial Velocity (m/s)**	**Mean Circumferential Velocity (m/s)**
Baseline	9.86×10^{-4}	-4.96	2.37
Porous Casing	8.26×10^{-4}	-2.10	0.72

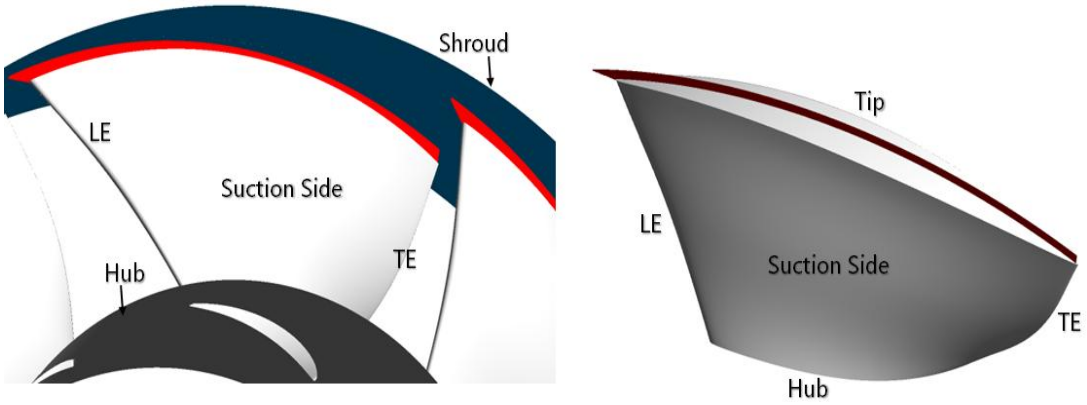

Fig. 16.Schematic of the plane (the 'Plane T') covering the whole gap over the blade tip (highlighted by red color).

In order to compare the evolution of TLV, the contours of vorticity on five selected planes (Plane 1 to Plane 5) are demonstrated in Fig. 17. These five planes are all produced nearly normal to the rotor tip chord direction. Moreover, the vorticity is the component being parallel to the tip chord direction. In Fig.17, TLV is detected as the region with extremely large absolute value of vorticity. When porous casing is employed, there is no obvious difference on the trajectory of the core of TLV.

However, the absolute strength of TLV decreases more significantly, as highlighted by red circles in Fig. 17 as an example. Moreover, both size and strength of the TLV released from the former adjacent blade (highlighted by black circles in Fig. 17) decreases when porous casing is applied. Detailed comparison of TLV on Plane 3 is given in Fig.18. Like Hah [46], TLV in the present study is found to be composed by the tip vortex ('TV' for short, with positive vorticity at the suction side) and the casing-boundary-layer-separation vortex ('CBSV' for short, with negative vorticity near the casing surface). CBSV is produced by the collision of two casing boundary layers: one forms with incoming main flow and the other is due to the reversed tip leakage flow. Then, CBSV moves away from casing surface and twines around the TV soon and the blockage effect of TLV is determined by both CBSV and TV. According to Fig. 18, porous casing obviously suppresses the strength of both CBSV and TV simultaneously, which is attributed to the reduced momentum of the flow in the casing boundary layer and the main flow in the fan tip gap.

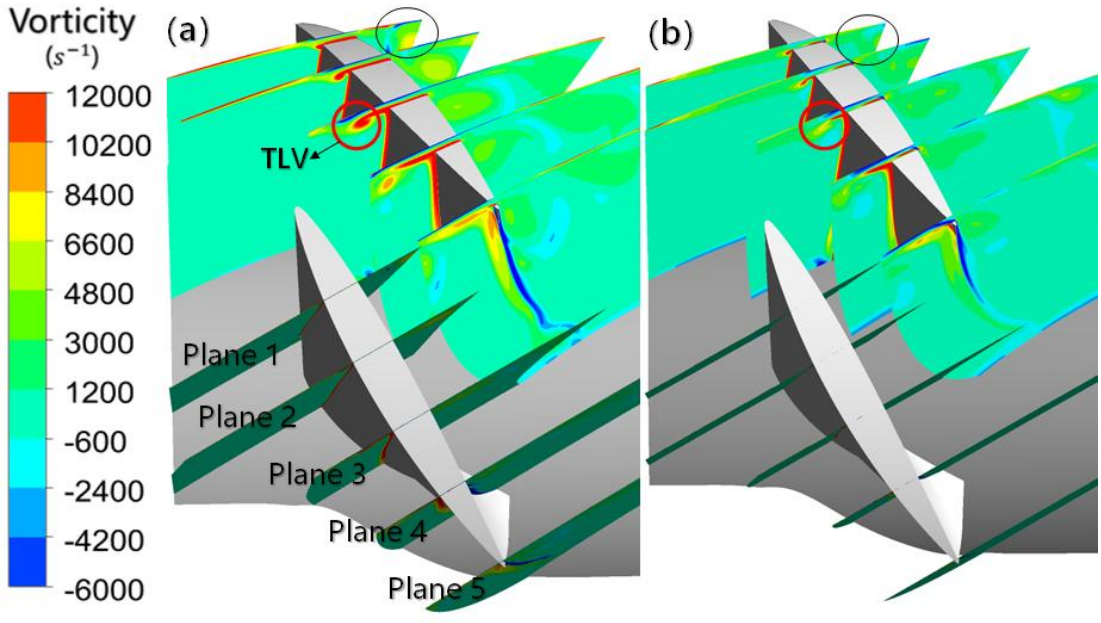

Fig. 17.Distribution of vorticity on selected planes (Plane 1 to Plane 5) normal to the rotor tip chord direction through the blade passage of (a) the baseline and (b) the fan with porous casing.

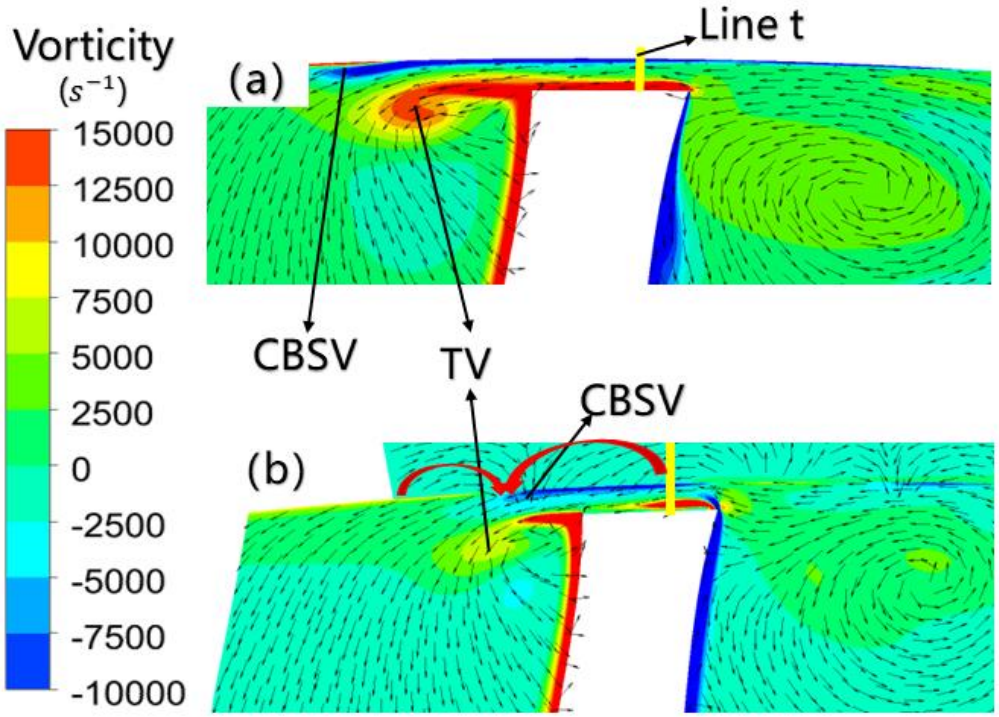

Fig. 18.Distribution of vorticity in the mid chord (Plane 3) for (a) the baseline and (b) the fan with porous casing. In the porous zone, the vectors of flow are produced according to the velocity in the stationary frame and their lengths are magnified.

Probable reasons for the decrease of tip flow momentum with open-cell porous casing include: (1) the reduction of pressure difference across the tip gap and (2) the momentum transport at fluid-porous interface. The former reason is supported by Fig. 19 which depicts the distribution of static pressure in the tip gap in both cases. The value of static pressure is captured on the intersection lines of the cylindrical surface (r=57.4mm) and the extension of pressure and suction surfaces of the fan blade ('PS' and 'SS', respectively in Fig. 19). It means that the driven forces (the static pressure difference) of the tip leakage flow for two cases are almost the same near the leading edge of the blade, while it is suppressed by the porous casing when the normalized chord length is in the range of 0.3 to 0.7. The momentum transport at fluid-porous interface is also very important. Actually, there are many academic works focusing on the flow near the fluid-porous interface [47-49]. Fig. 19 (b) gives the distribution of the axial velocity on the 'Line t' (shown in Fig. 18 (a)) for both fans. Compared with the baseline, with the porous casing, the magnitude of the axial flow velocity

decreases significantly out of the boundary layer on both the blade tip and the casing surface, leading to a reduced axial momentum of tip leakage flow. The velocity of flow at the rigid casing wall is zero due to no-slip boundary condition on casing. However, the velocity does not become zero at fluid-porous boundary (Radius=0.058 m) for the porous casing and it continues to decrease in the porous zone until reaching a small constant speed value. The observed effect of the metal foam on the distribution of axial flow velocity is consistent with the conclusion of the previous research [48].

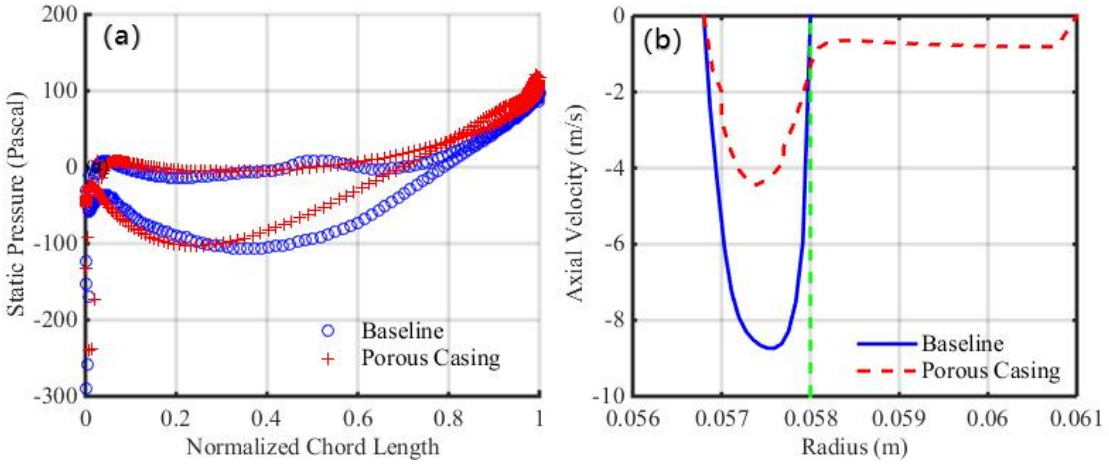

Fig. 19.Distribution of (a) the static pressure in the tip gap and (b) axial velocity on the Line t of two cases.

Being different from the present work, the most common explanation attributes the extending of fan stall margin to the flow "self-recirculation" in the extra channels because of casing treatment. It said that, driven by the pressure difference near the casing wall, fluid with high blockage and high pressure would be bled into the casing channels. Then, it re-injects at the casing to re-energize the low momentum fluid caused by TLV, leading to weaker blockage in the blade channel. Such explanation is presented by relevant studies focusing on the effect of traditional casing treatment method (using grooves or slots) [50-52]. Note that, although the above explanation is somehow reasonable, there is little detailed description for exact interaction between the 're-injected flow' and the flow of TLV. Especially, to the best of authors' knowledge, there is no rigorous quantitative analysis for the process of 're-energizing'

in the relevant studies. Therefore, there are also some works making their efforts to illustrate the effect of casing treatment in other ways [46,53]. It is really worth evaluating the effect of the 're-injected flow' on the change of original TLV, though it has not been completed in the present work.

5. Conclusions

The advantages of the open-cell porous casing on fan performance are firstly investigated experimentally. Then, the mechanism of porous casing is investigated through both experiments and numerical simulation. The results are summarized as follows:

(1) With constant tip clearance, the porous casing is experimentally proved to enhance the aerodynamic performance of the fan. It postpones stall inception to a lower flow rate and reduces the pressure loss during stall. Noise abatement is achieved at working conditions both before stall and during stall, especially during stall. The maximum noise reduction is greater than 10 dBA with fan speed adjustment.

(2) The effect of rough casing surface is tested by attaching abrasive paper on the casing inner wall. It reveals that the rough casing surface makes slight improvement on fan aerodynamic performance. However, it cannot help to decrease the total noise as porous casings do. Porous material attached is supposed to absorb the radiated noise directly, but this effect is negligible due to its limited volume.

(3) Taking advantage of the original pressure difference in rotor blade row, porous casing reduces the high momentum of tip leakage flow and the present study attributes it to the release of the high pressure difference between the pressure side and suction side of the blade and the momentum transport at fluid-porous interface. The strength of the tip leakage vortex decreases, which is beneficial to the delay of stall inception and noise suppression.

ACKNOWLEDGMENT

The first author acknowledges the support of the Ph.D. studentship from the University of Hong Kong. He also thanks Mr. Zhenjiang Zhan, a senior research assistant in MIDEA, for his kindly help on the measurement of flow resistance of the metal foam in the present study.

REFERENCES

[1] Moreau, S., 2019, “Turbomachinery Noise Predictions: Present and Future,” Acoustics, 1, pp. 92-116.

[2] Moreau, S., Roger, M., 2007, “Competing Broadband Noise Mechanisms in Low-speed Axial Fans,” AIAA J., **45**(1), pp.48-57.

[3] Longhouse, R. E., 1978, “Control of Tip-Vortex Noise of Axial Flow Fans by Rotating Shrouds,” J. Sound Vib.,**58**(2), pp. 201-214.

[4] Dittmar, J. H, 1977, "Interaction of Rotor Tip Flow Irregularities with Stator Vanes as a Noise Source," 4th Aeroacoustics Conference, Atlanta, GA.

[5] Schaub, U. W., Vlasic, E., and Moustapha, S. H., 1993, “Effect of Tip Clearance on the Performance of a Highly Loaded Turbine Stage,” Technology Requirements for Small Gas Turbine, AGARD CP-537, 1993, Paper 29.

[6] Kameier, F., and Neise, W., 1997, “Experimental Study of Tip Clearance Losses and Noise in Axial Turbomachines and Their Reduction,” ASME J. Turbomach., **119**(3), pp. 460-471.

[7] Corsini, A., Rispoli, F., and Sheard, A. G., 2010, “Shaping of Tip End-Plate to Control Leakage Vortex Swirl in Axial Flow Fans,” ASME J. Turbomach., **132**(3), p. 031005.

[8] Cai, Y. J., Zhong, Y. L., Qian, L. H., He, S. Z., and Pang, Q. H., 1985, “Increasing Surge Margin in an Axial Flow Compressor Using End-Bend Airfoils,” ASME 1985 Beijing International Gas Turbine Symposium and Exposition. American Society of Mechanical Engineers, 1985: V001T02A009-V001T02A009.

[9] Ye, X., Li, P., Li, C., and Ding, X., 2015, “Numerical investigation of blade tip grooving effect on performance and dynamics of an axial flow fan,” Energy, 82, pp. 556-569.

[10] Khorrami, M. R., Li, F., and Choudhari, M., 2002, “Novel approach for reducing rotor tip-clearance-induced noise in turbofan engines,” AIAA J., **40**(8), pp. 1518-1528.

[11] Moore, R. D., Kovich, G., and Blade, R. J., 1971, “Effect of Casing Treatment on Overall and Blade-Element Performance of a Compressor Rotor,” NASA TN D-6538.

[12] Takata, H., and Tsukuda, Y., 1977, “Stall Margin Improvement by Casing Treatment—Its Mechanism and Effectiveness,” J. Eng. Power, **99**, pp. 121– 133.

[13] Crook, A. J., Greitzer, E. M., Tan, C. S., and Adamczyk, J. J., 1993, "Numerical Simulation of Compressor Endwall and Casing Treatment Flow Phenomena," ASME J. Turbomach., **1153**(3), pp. 501–512.

[14] Fujita, H., and TAKATA, H., 1984, "A Study on Configurations of Casing Treatment for Axial Flow Compressors," Bulletin of JSME, **27**(230), pp. 1675-1681.

[15] Smith, G. D. J., and Cumpsty, N. A., 1984, "Flow Phenomena in Compressor Casing Treatment," ASME J. Eng. Gas Turbines Power, **106**(3), pp. 532-541.

[16] Sutliff, D.L., and Jones, M., 2008, "Foam-Metal Liner Attenuation of Low-Speed Fan Noise," 14th AIAA/CEAS Aeroacoustics Conference (29th AIAA Aeroacoustics Conference), British Columbia, Canada.

[17] Sutliff, D. L. and Jones, M. G., 2009, "Low-Speed Fan Noise Attenuation from a Foam-Metal Liner," Journal of Aircraft, **46**, pp. 1381-94.

[18] Sutliff, D. L., Jones, M. G., Hartley, T. C., 2013, "High-Speed Turbofan Noise Reduction Using Foam-Metal Liner Over-the-Rotor," Journal of Aircraft, **50**, pp. 1491-503.

[19] Xu, C., and Mao, Y., 2016, "Passive Control of Centrifugal Fan Noise by Employing Open-Cell Metal Foam," Appli. Acoust.,**103**, pp. 10-19.

[20] You, D., Wang, M., Moin, P., and Mittal, R., 2006, "Effects of Tip-gap Size on the Tip-leakage flow in a Turbomachinery Cascade," Physics of Fluids, **18,** 105102.

[21] Lu, X., Chu, W., Zhang, Y., and Zhu, J., 2006, "Experimental and Numerical Investigation of a Subsonic Compressor with Bend-Skewed Slot-Casing Treatment," Proceedings of the Institution of Mechanical Engineers, Part C: Journal of Mechanical Engineering Science, **220**(12), pp. 1785-1796.

[22] Magne, S., Sanjose, M., Moreau, S., and Berry, A., 2012, "Aeroacoustic Prediction of the Tonal Noise Radiated by a Ring Fan in Uniform Inlet Flow," 18th AIAA/CEAS Aeroacoustics Conference (33rd AIAA Aeroacoustics Conference), Colorado Springs, United States of America.

[23] Wang, G., Duchaine, F., Papadogiannis, D., Duran, I., Moreau, S., and Gicquel, L., 2014, "An Overset Grid Method for Large Eddy Simulation of Turbomachinery Stages," Journal of Computational Physics, **274**, pp. 333-355.

[24] Jiang, C., Yauwenas, Y., Fischer, J., Moreau, D., Doolan, Con., Gao, J., Jiang, W., McKay, R., and Kingan, M., 2018, "Control of Rotor Trailing Edge Noise Using Porous Additively Manufactured Blades," 2018 AIAA/CEAS Aeroacoustics Conference, Atlanta, Georgia, United States of America.

[25] Leonard, T., Sanjose, M., Moreau, S., and Duchaine, F., 2019, "Large Eddy Simulation of a Scale-Model Turbofan for Fan Noise Source Diagnostic," J. Sound Vib.,**445**, pp. 64-76.

[26] Moreau, S., and Sanjose, M., 2016, "Sub-harmonic Broadband Humps and Tip Noise in Low-speed Ring Fans," J. Acoust. Soc. Am., **139**(118), pp. 118-127.

[27] Wang, C., 2016, "Noise Source Analysis and Control for Small Axial-Flow Fans," Ph.D. dissertation, the University of Hong Kong, Hong Kong, China.

[28] Tyler, J. M., and Sofrin, T. G., 1962, "Axial Flow Compressor Noise Studies," Soc. Autom. Eng. Trans., **70**, pp. 309-332.

[29] Huang, L., 2003, "Characterizing Computer Cooling Fan Noise," J. Acoust. Soc. Am., **114**, pp. 3189-3200.

[30] Wang, J., and Huang, L., 2006, "Quantification and Control of Noise Sources In a Small Axial-Flow Fan," Noise Control Engineering Journal, **54**(1), pp. 27-32.

[31] Wang, C., 2018, "Noise Source Analysis for Two Identical Small Axial-flow Fans in Series under Operating Condition," Appl. Acoust., **129**, pp. 13-26.

[32] ANSI/AMCA Standard 210, 1999, Laboratory Method of Testing Fans for Aerodynamic Performance Rating, Air Movement and Control Association International, Inc. and American Society of Heating, Refrigerating and Air Conditioning Engineers, Inc., Illinois, USA.

[33] Utsuno, H., Tanaka, T., Fujikawa, T., and Seybert, A. F., 1989, "Transfer Function Method for Measuring Characteristic Impedance and Propagation Constant of Porous Materials," J. Acoust. Soc. Am., **86**(2), pp. 637-643.

[34] Delany, M. E., and Bazley, E. N., 1970, "Acoustical Properties of Fibrous Absorbent Materials," Appli. Acoust., **3**(2), pp. 105-116.

[35] Turkel, E., and Yefet, A., 1998, "Absorbing PML Boundary Layers for Wave-Like Equations," Appl. Numer. Math., **27**(4), pp. 533-557.

[36] Biot M. A., 1956, "Theory of Propagation of Elastic Waves in a Fluid-Saturated Porous Solid. I. Low-frequency Range," J. Acoust. Soc. Am., **28**, pp. 168-78.

[37] Jiang, C., Wang, C. and Huang, L., 2019, "Acoustic Characterization of Ducts Lined with Poroelastic Materials Based on Wave Finite Element Method," Appl. Acoust., **145**, pp. 362-373.

[38] Rao, N., Kavurmacioglu, L., Gumusel, B. and Camci, C., 2006, Influence of Casing Roughness on the Aerodynamic Structure of Tip Vortices in an Axial Flow Turbine, ASME Paper GT2006-91011, presented at the ASME International Gas Turbine Congress in Barcelona, Spain.

[39] ANSYS CFX 11.0 Reference Guide, ANSYS Inc., 2006.

[40] Bernicke, P., Akkermans, R., Ananthan, V., Ewert, R., Dierke, J., and Rossian, L., 2019, "A Zonal Noise Prediction Method for Trailing-edge Noise with a Porous Model," International Journal of Heat and Fluid Flow, 80, 108469.

[41] Jeng, T. M., and Tzeng, S. C., 2005, "A semi-empirical model for estimating permeability and inertial coefficient of pin-fin heat sinks," International journal of heat and mass transfer, **48**(15), pp. 3140-3150.

[42] Mancin, S., Zilio, C., Cavallini, A., and Rossetto, L., 2010, "Pressure drop during air flow in aluminum foams," International Journal of Heat and Mass Transfer, **53**(15-16), pp. 3121-3130.

[43] Lee, K. Y., Choi, Y. S., Kim, Y. L., and Yun, J. H., 2008, "Design of Axial Fan Using Inverse Design Method," J. Mech. Sci. Technol., **22**, pp. 1883–1888.

[44] Jian, H., and Hu, W., 2008, "Numerical Investigation of Inlet Distortion on an Axial Flow Compressor Rotor with Circumferential Groove Casing Treatment," Chinese Journal of Aeronautics," **21**(8), pp. 496-505.

[45] Wilke, I., and Kau, H.-P., 2003, "A Numerical Investigation of the Flow Mechanisms in a HPC Front Stage with Axial Slots", Proceedings of ASME Turbo Expo 2003, June 16- 19, Atlanta, Georgia, USA, paper GT-2003-38481

[46] Hah, C., 2018, "The Inner Workings of Axial Casing Grooves in a One and a Half Stage Axial Compressor with a Large Rotor Tip Gap: Changes in Stall Margin and Efficiency", Proceeding of ASME Turbo Expo 2018, Turbomachinery Technical Conference and Exposition, June 11-15, Osio, Norway, GT2018.

[47] Beavers, G. S., and Joseph, D. D., 1967, "Boundary Conditions at a Naturally Permeable Wall," J. Fluid Mech., **30**(1), pp. 197-207.

[48] Goyeau, B., Lhuillier, D., Gobin, D., and Velarde M. G., 2003, "Momentum Transport at a Fluid–Porous Interface," Intl J. Heat Mass Trans, **46**(21), pp. 4071-4081.

[49] Ochoa-Tapia, J., and Whitaker, S., 1995, "Momentum Transfer at the Boundary between a Porous Medium and a Homogeneous Fluid: I-Theoretical Development," Int. J. Heat Mass Transf. **38**, pp. 2635–2646.

[50] Hathaway, M. D., 2002, "Self-Recirculating Casing Treatment Concept for Enhanced Compressor Performance", Proceedings of ASME Turbo Expo 2002, June 3-6, Amsterdam, The Netherlands, paper GT-2002-30368.

[51] Iyengar, V., Sankar, L., and Niazi, S., 2005, "Assessment of the Self Recirculating Casing Treatment Concept to Axial Compressors," AIAA Paper No. 2005-0632.

[52] Qiang, X. Q., Zhu, M. M., and Teng, J. F., 2013, "Effect of Circumferential Grooves Casing Treatment on Tip Leakage Flow and Loss in a Transonic Mixed-Flow Compressor," Journal of Theoretical and Applied Mechanics, **51**(4), pp. 903-913.

[53] Lin, F., Ning, F., and Liu, H., 2008, "Aerodynamics of Compressor Casing Treatment: Part I—Experiment and Time-Accurate Numerical Simulation", ASME Turbo Expo 2008: Power for Land, Sea, and Air. American Society of Mechanical Engineers, 2008: 731-744.